Dynamics of coal fire in Jharia Coalfield, Jharkhand, India during the 1990s as observed from space

R. S. Chatterjee[1,*], Md. Wahiduzzaman[2], Ankit Shah[1], E. V. R. Raju[3], R. C. Lakhera[1] and V. K. Dadhwal[1]

[1]Indian Institute of Remote Sensing, Dehradun 248 001, India
[2]Geological Survey of Bangladesh, Dhaka 1000, Bangladesh
[3]Bharat Coking Coal Limited, Dhanbad 826 005, India

Jharia Coalfield in Jharkhand, India, is known for being the exclusive storehouse of prime coking coal in the country. The coalfield is also known for hosting the maximum number of known coal fires among all coalfields in India. In the present investigation, an attempt was made to study the coal fire dynamics of Jharia Coalfield during the 1990s from medium resolution satellite thermal IR data such as Landsat-5 TM and Landsat-7 ETM+ data (acquired in 10.4–12.5 μm spectral region). The dynamics of coal fire was addressed on the two following aspects: (i) changes in the spatial extent of fire-affected areas, and (ii) propagation of coal fire during the 1990s. A marked decrease in the spatial extent of fire-affected areas during the 1990s was observed in this study. The spatial coverage of surface and subsurface coal fires was found to change from 0.42 and 2.06 km^2 respectively, in 1992, to 0.33 and 1.36 km^2 respectively, in 1996 and 0.08 and 1.60 km^2 respectively, in 2001. Using the three available satellite thermal datasets acquired in 1992, 1996 and 2001, an attempt was made to find the net lateral propagation during 1992–96 and 1996–2001. The propagation of coal fire was found to be more erratic than regular in nature. During 1992–96, the net lateral propagation was in general towards south and at places towards west, whereas during 1996–2001 it was in general towards north.

Keywords: Coal fire, dynamics, Jharia coalfield, satellite thermal data.

THE temperature anomaly of the earth's surface due to surface and subsurface coal fires can be mapped by sensing the thermal radiation emitted from the earth's surface. Planck's blackbody radiation equation relates spectral radiance and wavelength with radiant temperature of an object as follows:

$$L_\lambda = \frac{2hc^2\lambda^{-5}}{e^{\frac{hc}{\lambda k T_{rad}}} - 1}, \quad (1)$$

where L_λ is the spectral radiance (in W/m^2/sr/μm).

Equation (1) can be rearranged as follows:

$$T_{rad} = \frac{hc/k}{\lambda \ln\left[\frac{2hc^2\lambda^{-5}}{L_\lambda} + 1\right]}. \quad (2)$$

In eq. (2), wavelength may be considered as the mean of the spectral region under investigation (e.g. 11.45 μm in Landsat TM and ETM+ band 6 data). Given the spectral radiance, the radiant temperature of a pixel can be calculated using eq. (2). When spectral emissivity (ε_λ) of a pixel is available, kinetic temperature of the said pixel may be obtained using the following mathematical relation:

$$T_{kin} = \frac{1}{\varepsilon_\lambda^{1/4}} T_{rad}. \quad (3)$$

Spectral radiance in individual bands may be calculated from the satellite data using the calibration parameters of each band. Markham and Barker[1] listed post-calibration dynamic range of Landsat TM thermal IR data (10.4–12.5 μm) for calculating spectral radiance from digital numbers of Landsat TM digital data. Many of the previous workers[2–5] have used these cut-off values (of the dynamic range). Temperature of the fire pixels obtained by this procedure was found to be quite low, which appears unrealistic, particularly in areas where surface fire occupies reasonably wider areal extent of the pixels. In this work, instead of using standard calibration parameters such as the listed post calibration dynamic range of Markham and Barker[1], we have used scene-specific calibration parameters such as gain and offset of the detectors in each band. Because of high gain settings, the thermal IR sensors in Landsat-5 TM and Landsat-7 ETM+ get saturated at approximately 70 and 75°C respectively.

Our study area, the Jharia Coalfield, is located near Dhanbad town, which is 260 km northwest from Kolkata and 1150 km southeast from Delhi (Figure 1 *a*). The coalfield is bounded by lat. 23°35′–23°55′N and long. 86°05′–

*For correspondence. (e-mail: rschatterjee@iirs.gov.in)

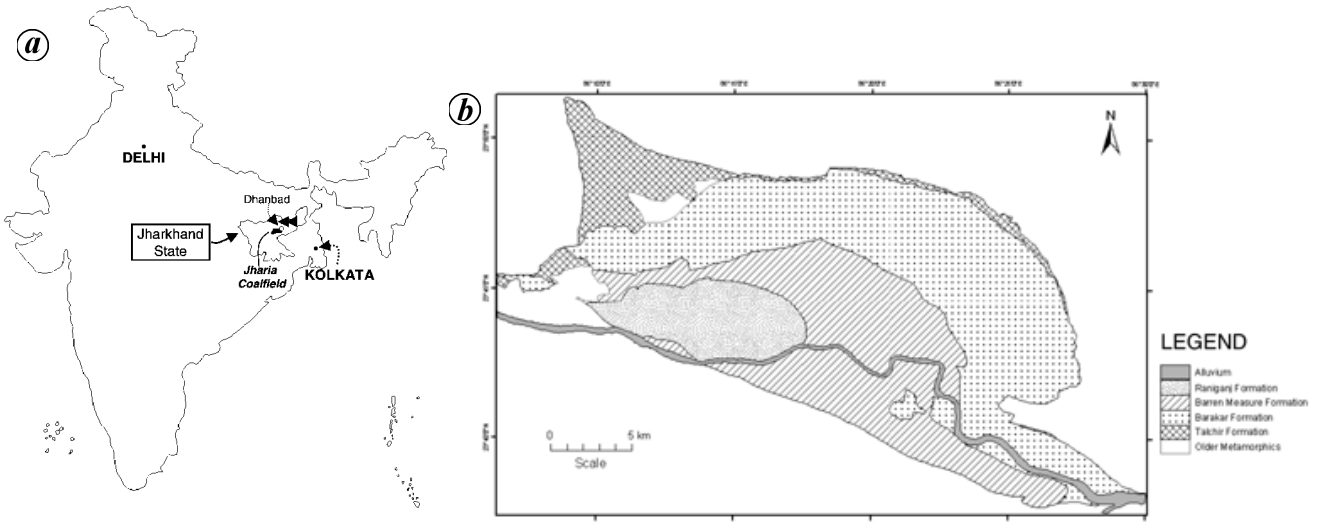

Figure 1. ***a***, Location of Jharia Coalfield, Jharkhand, India. ***b***, Spatial disposition of stratigraphic units showing configuration of coal-bearing formations (after GSI[15]).

86°30′E approximately and covers an areal extent of ~450 sq. km. The major coal-bearing formation in Jharia Coalfield, the Barakar Formation of Early Permian age, forming a sickle-shaped outline in the northern part of the coalfield (Figure 1 *b*), is severely fire-affected.

From the kinetic temperature image of Jharia Coalfield, surface and subsurface coal-fire pixels may be delineated based on the appropriate threshold temperatures for surface and subsurface coal-fire mixed pixels. Approximate threshold temperature for differentiating surface and subsurface fire pixels may be obtained from the field-based modelling of pixel-integrated temperature[6] or by simple trial and error, aided by the field occurrences of surface and subsurface coal fires.

From multi-date coal fire maps, changes in the spatial extent of coal fire and propagation of coal fire were attempted in this study. Various factors are responsible for the propagation of coal fire, namely three-dimensional disposition of the affected coal seam; presence of neighbouring coal seams, coal debris accumulation and coal-bearing overburden dumps; density and orientation of the fractures, their depth consistency, and occurrences of opencast mines, particularly the waterlogged closed/abandoned opencast mines which may act as discontinuities to fire propagation. It appears to be more feasible to obtain the direction of lateral propagation than the direction of vertical propagation from multi-date satellite thermal data. However, coal-fire propagation is more a path function than a state function between two discrete observations at different times. Large time series satellite data with sufficiently dense temporal sampling are therefore essential for coal-fire propagation studies. It may be feasible only to obtain the net lateral propagation of coal fire from a handful (say, 2 or 3) of satellite datasets. Moreover, meteorological parameters at the time of data acquisition, namely wind speed and direction, have significant influence in coal-fire propagation studies as they affect the spread of surface fire.

Data used

In this study, we have used night-time Landsat-5 TM thermal infrared (TIR) and shortwave infrared (SWIR) data of 9 March 1992 and 21 April 1996, and day-time Landsat-7 ETM+ TIR data of 2 November 2001.

Night-time thermal data were preferred to avoid the solar heating component of the total radiant energy flux from the earth's surface and particularly the differential solar heating component due to topographic unevenness of the terrain. Moreover, in the case SWIR data (e.g. Landsat TM/ETM+ band 7; data acquired in the 2.08–2.35 μm spectral region), which are potentially used for the identification of surface coal fires[4,7,8], it is difficult to separate and remove the reflected energy component from the thermal radiation component in day-time data. Due to non-availability of night-time Landsat-7 ETM+ data, we have worked with day-time Landsat-7 ETM+ TIR data only.

Methodology

From the night-time Landsat-5 TM raw digital data of March 1992 and April 1996 and day-time Landsat-7 ETM+ raw digital data of November, 2001, spectral radiance (L_λ) for each pixel of the three datasets was calculated using scene-specific average calibration parameters (gain and offset) as described below[6]:

$$L_\lambda = \frac{\text{DSL} - \text{Offset}_{\text{Ave}}}{\text{Gain}_{\text{Ave}}} \quad (4)$$

where DSL and $Offset_{Ave}$ represent digital signal level of the said pixel and average offset digital signal level of the given band respectively, in $W/m^2/sr/\mu m$, and $Gain_{Ave}$ is the average gain coefficient of the given band. Spectral radiance thus calculated represents at-satellite or top-of-atmosphere spectral radiance. At-satellite spectral radiance needs to be corrected from atmospheric effects[9–11]. In the absence of aerosol size-distribution profile, transmittance and path radiance estimated from the standard atmosphere and aerosol models[12] supplied by LOWTRAN 7 was not found to improve the results in case of Jharia Coalfield[10].

Using mean wavelengths of the spectral regions under investigation, e.g. 11.45 and 2.215 μm for Landsat-5 TM and Landsat-7 ETM+ bands 6 and 7 respectively, and spectral radiance values, radiant temperature at each pixel of the three datasets was calculated using the Planck's radiation equation (eq. (2)). From radiant temperature, kinetic temperature may be calculated by supplying thermal emissivity of the corresponding pixels (eq. (3)). Thermal emissivity for each ground resolution cell or pixel of satellite TIR data was calculated by knowledge-based approach: from NDVI (normalized difference vegetation index) values in vegetation covered areas (with NDVI > 0) and from the knowledge of spectral absorption properties of surface materials in areas devoid of vegetation (NDVI ≤ 0). In this study, medium resolution optical multispectral satellite data (NIR and red-band data) from Landsat-5 TM, IRS 1C LISS-III and Landsat-7 ETM+ sensors were used to derive areally-representative NDVI values for the corresponding TIR data. From the satellite-based NDVI values, thermal emissivity (ε) was calculated using the following empirical equation[13]:

$$\varepsilon = a + b * \ln(\text{NDVI}), \quad (5)$$

where a and b are two constants (a = 1.0094 and b = 0.047 for a correlation coefficient of 0.941 at 0.01 level of significance).

However, in coal fire-mapping application, fire-affected areas are mostly devoid of vegetation. For areas covered by coal or water, the value of thermal emissivity was considered 1.0 due to their ability to absorb thermal radiations almost completely. For areas covered by rocks, presumably sandstone and shale, loose sand deposits or bare soil, the value of thermal emissivity[14] was considered 0.92.

Subsequently, by field-based modelling of pixel-integrated temperature for Landsat-5 TM TIR data, tentative threshold temperature of typical surface fire mixed pixels could be determined as ~54 and ~56°C respectively, for March 1992 and April 1996 data[6]. This is corroborated by the field occurrences of surface coal fire mixed pixels. The threshold temperature between subsurface coal fire and non-fire areas was determined based on the temperature of coal-covered areas without fire and urban clusters in the TIR temperature images. It is observed that 48 and 50°C respectively, are good approximation as threshold pixel-integrated temperature values for night-time March 1992 and April 1996 data. The tentative threshold temperatures for surface and subsurface coal fire pixels in the kinetic temperature image derived from day-time Landsat ETM+ data of 2001 was determined based on the field occurrences of surface and subsurface coal-fire pixels.

Attempts were made to identify surface coal fire locations more definitively from night-time SWIR data such as Landsat-5 TM band 7 (2.08–2.35 μm) data. The temperature sensitivity of Landsat-5 TM band 7 (160–277°C)[8] broadly matches with the surface coal-fire temperature range (150–250°C). Moreover, it does not get saturated at ~70°C unlike the thermal band. Also, due to its higher spatial resolution (30 m compared to 120 m in Landsat-5 TM thermal band), detection of surface coal-fire pixels is facilitated. Radiant temperature images were generated from night-time Landsat-5 TM band 7 data of 1992 and 1996. Thresholding of surface-fire pixels from background noise was done at 150°C and above.

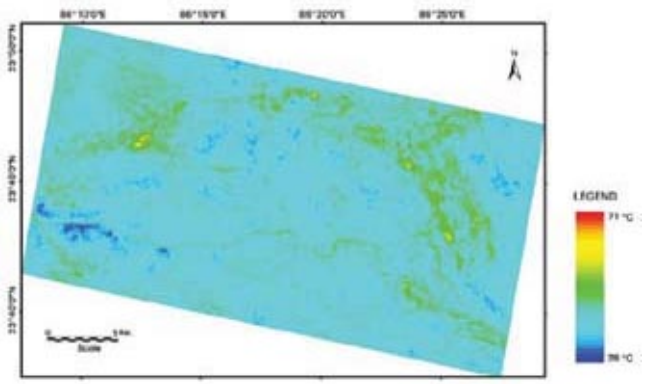

Figure 2. Radiant temperature image of Jharia Coalfield generated from night-time Landsat-5 TM band 6 data of March 1992.

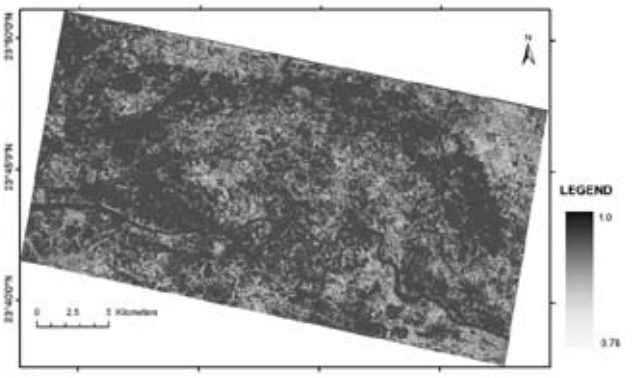

Figure 3. Knowledge-based thermal emissivity image of Jharia Coalfield.

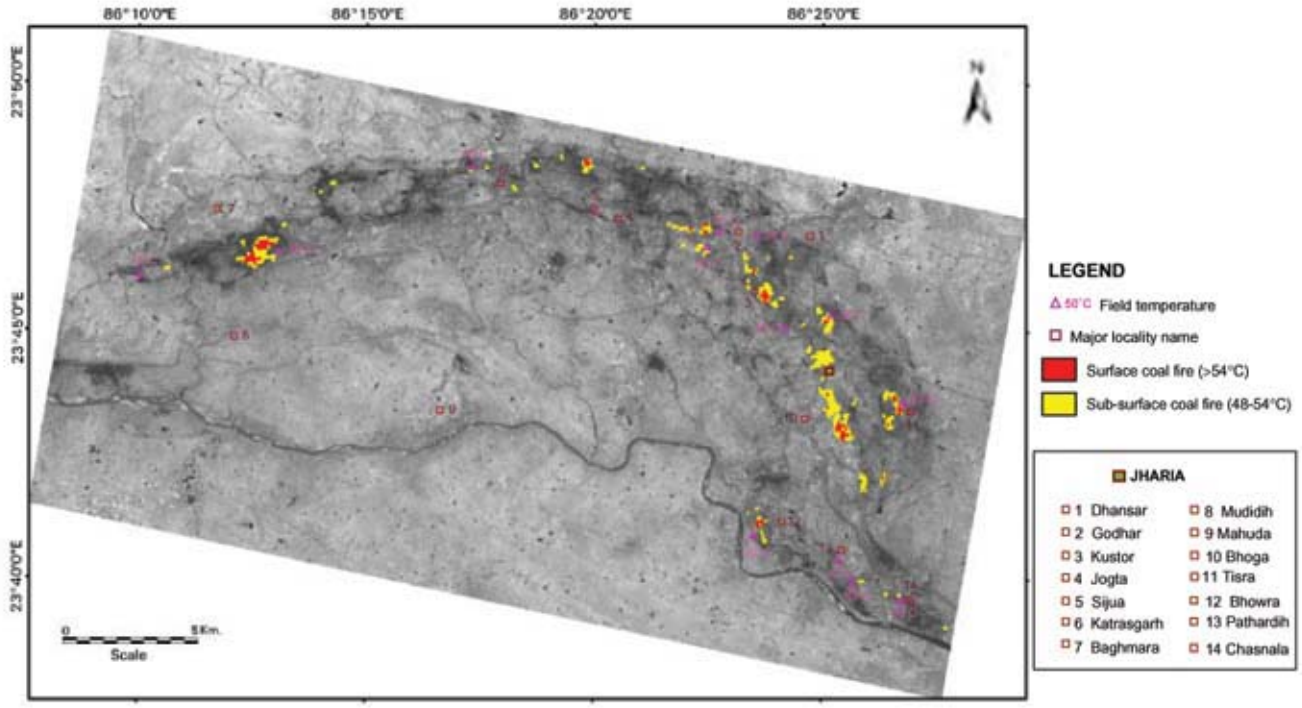

Figure 4. Surface and subsurface coal-fire areas of Jharia Coalfield during 1992 obtained from night-time Landsat-5 TM band 6 data and field-based modelling of pixel-integrated temperature for surface coal fire. (Overlain on IRS LISS-3 NIR image.) Field temperature at selective locations measured by IR thermometer during similar time of the year in 2003 are shown for validation of results.

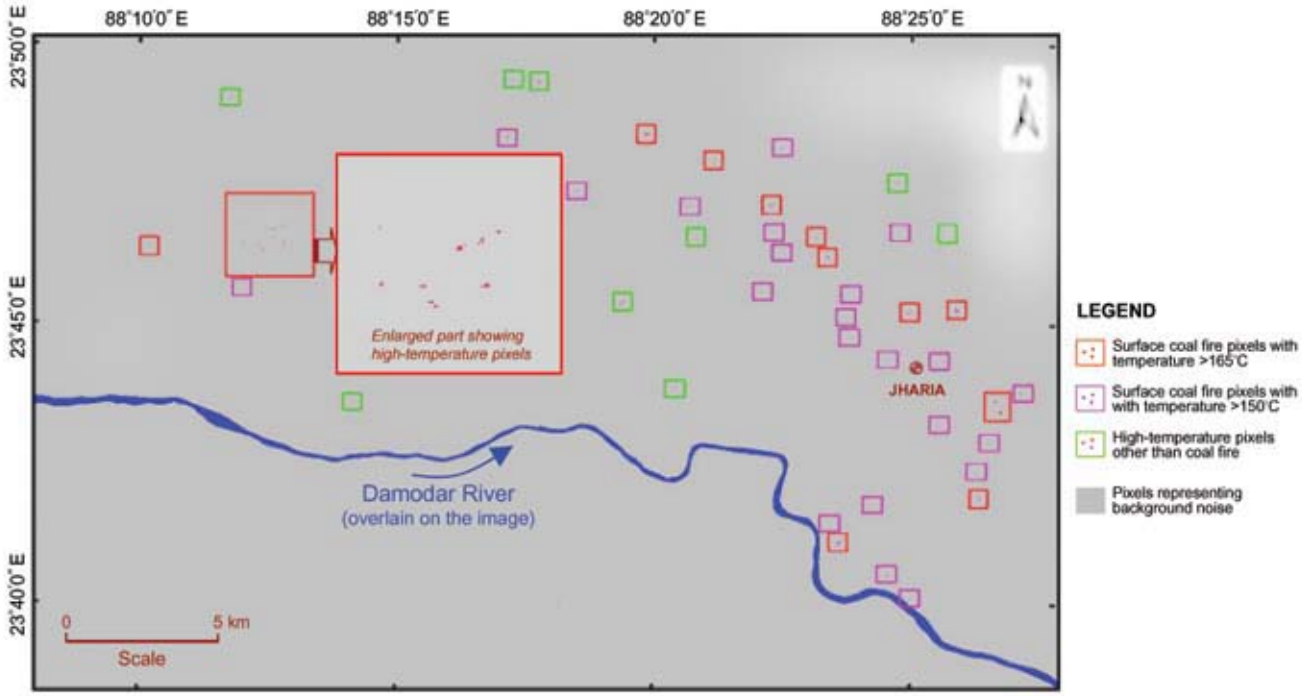

Figure 5. Surface coal-fire pixels (outlined by red and purple rectangles) are precisely identified from night-time Landsat-5 TM band 7 data of Jharia Coalfield acquired in 1992.

Results and discussion

From the night-time Landsat-5 TM data of 1992 and 1996 and day-time Landsat-7 ETM+ data of 2001, the spectral radiance images were generated using scene-specific calibration parameters, such as average gain and offset of the individual scenes. From the spectral radiance images, radiant temperature images were generated subsequently using Planck's radiation equation (Figure 2). Thermal emissivity values were calculated corresponding to the thermal image pixels based on NDVI values obtained from optical multispectral data in NIR and red bands (where NDVI > 0) or spectral absorption properties of the surface materials (NDVI ≤ 0; Figure 3). Using radiant temperature and thermal emissivity values, kinetic temperature images were generated corresponding to Landsat-5 TM band 6 data of 1992 and 1996 and Landsat-7 ETM+ band 6 data of 2001. Subsequently, by thresholding the kinetic temperature range, on the basis of field-based modelling of surface coal fire mixed pixel temperature and field occurrences of surface coal-fire, surface and subsurface coal fire pixels were delineated (Figure 4). Moreover, from the night-time Landsat-5 TM band 7 data of 1992 and 1996, surface fire locations were pinpointed (Figure 5). Surface fire pixels could be easily discriminated by simple thresholding of high-temperature pixels. Two threshold temperatures, 150 and 165°C were chosen broadly based on the frequency distribution of the high-temperature pixels.

The spatial coverages of surface and subsurface coal fires were found to be 0.42 and 2.06 sq. km respectively, in 1992; 0.33 and 1.36 sq. km respectively, in 1996 and 0.08 and 1.60 sq. km respectively in 2001 (Table 1, Figure 6). The study shows that the spatial coverage of surface coal fire was reduced to a great extent during 1992–2001. Similarly, the spatial coverage of subsurface coal fire was reduced in general during the observation period. Although during 1992–1996, subsurface coal-fire was reduced substantially, it showed minor increase during 1996–2001. The total coal fire-affected area in Jharia Coalfield (including surface and subsurface fires) was found to decrease from 2.49 sq. km in 1992, to 1.70 sq. km in 1996 and to 1.59 sq. km in 2001, which accounts for a decrease of ~32% during 1992–96 and ~6.5% during 1996–2001.

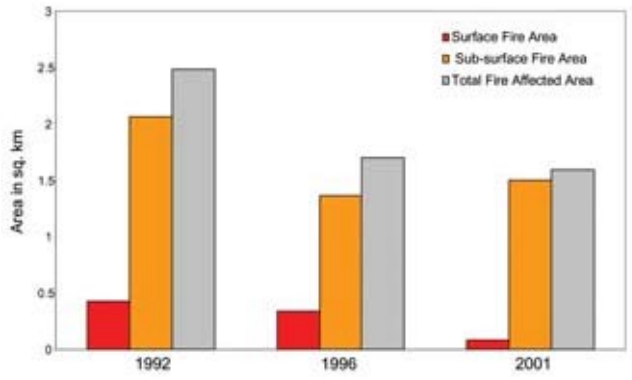

Figure 6. Bar diagram showing changes in spatial extent of surface, subsurface and total fire-affected areas in Jharia Coalfield in 1992, 1996 and 2001.

Decrease in the spatial extent of coal fire might have occurred due to several reasons as described below.

(i) Various reclamation measures were adopted by Bharat Coking Coal Limited (BCCL), Dhanbad for arresting coal fire and restricting the propagation of fire:
(a) Removal of fire-affected coal seams, particularly the fire-affected portions of the affected coal seams from the unaffected coal seams by selective opencast mining operations.
(b) Dumping of the fire-affected portions of the affected coal seams and overburden dumps at a safe place to let them burn out naturally and completely.
(c) Surface blanketing by incombustible materials, e.g. fly-ash, soil and sand followed by dozing, compaction and dense plantation. Over 22 million cubic metre of surface blanketing work has been carried out so far by BCCL for combating coal fire.
(d) Quenching coal fire by water-pooling of fire-affected opencast quarries to extinguish/alleviate fire from the affected portions.
(e) Isolation of fire by trenching around the fire-affected coal seams.
(f) Isolation of fire by construction of sand/cement grout cut-off barriers.
(g) Hydraulic stowing/blind flushing through boreholes. More than 50 million cubic metre of sand has been stowed below ground.
(h) Infusion of inert gas. Over 3 million cubic metre of nitrogen gas has been flushed below the ground to control fires.

(ii) Besides, in many of the age-old coal fires, coal or coaliferous hydrocarbon matter required for burning might have been exhausted due to continuous and uncontrolled burning over a period of time (Figure 7).

On the other hand, several new fire sites came into existence during the observation period or afterwards, due to vertical and/or lateral propagation of the subsurface fire to the surface (Figure 8 *a*) or incidence of fresh fire from underground mining galleries with the progress of new opencast mining activities (Figure 8 *b*). In some places, fire-affected sites were abandoned and mining operations were stopped completely, which led to uncontrolled growth of fire in and around the given sites (Figure 8 *c*).

The direction of coal-fire propagation is an important input for arresting and controlling coal fire. Propagation of coal fire is more a path function than state function be-

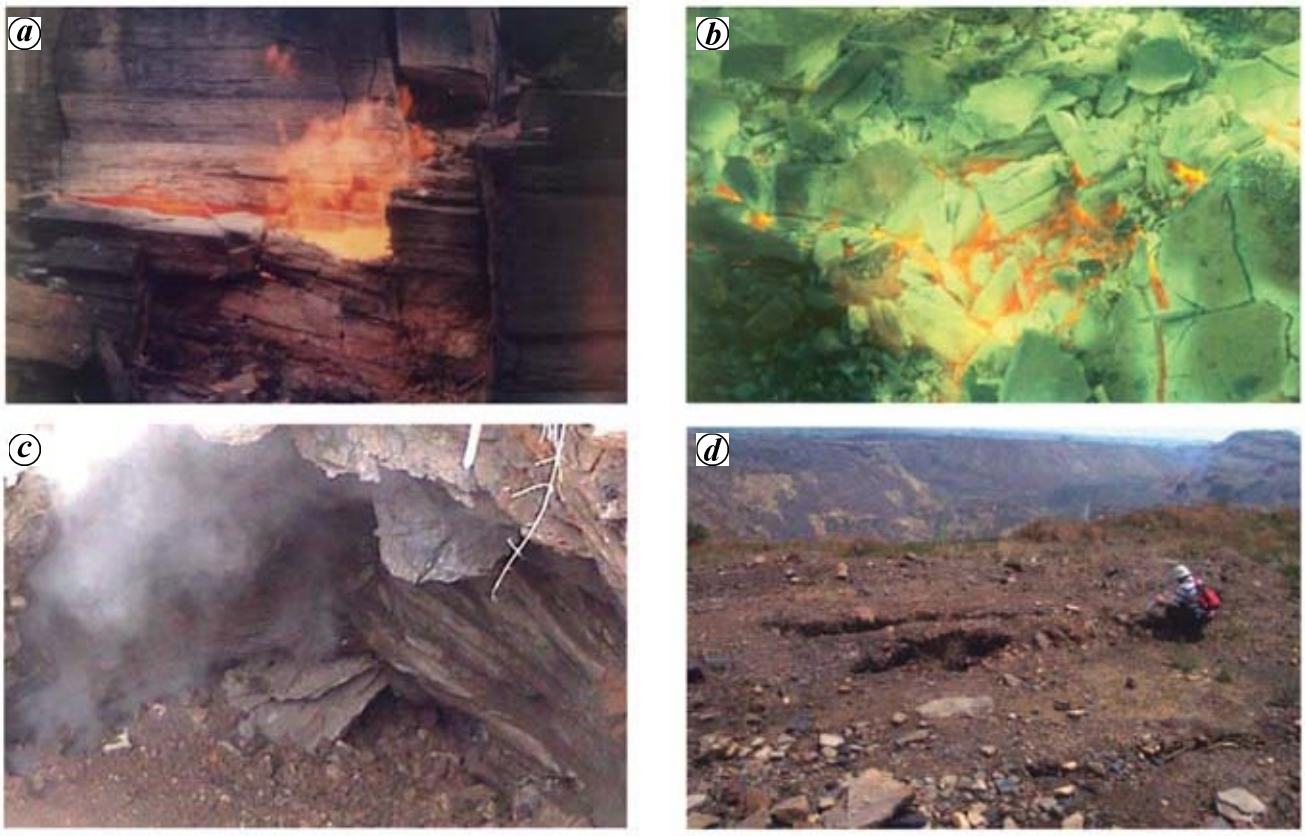

Figure 7. Subsided seam fire (***a*** and ***c***) and debris fire (***b*** and ***d***) at Rajapur, near Jharia town. Photographs (***a***) and (***b***) were taken in 1992 whereas photographs (***c***) and (***d***) were taken in 2005 from the same sites but different spots. Photographs are representative of the scenario.

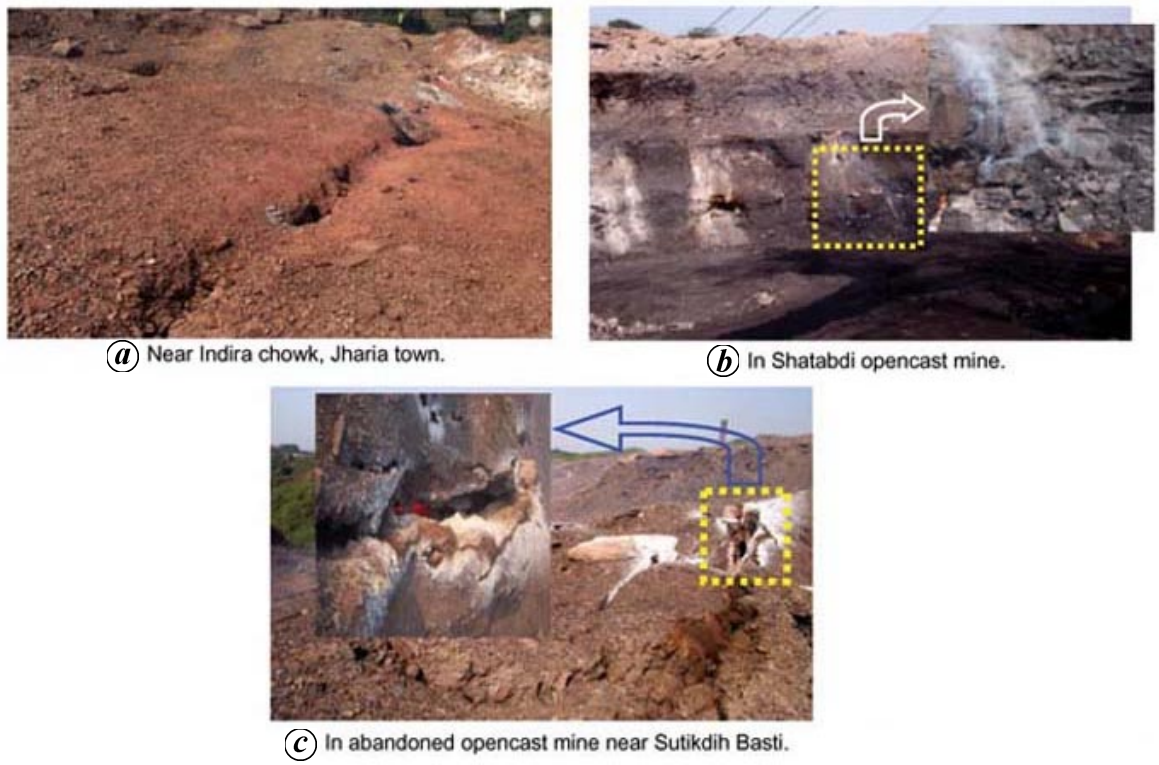

Figure 8. Incidence of fresh surface fire due to vertical propagation of subsurface fire to the surface (***a***), from underground mining galleries with the progress of new opencast mining activities (***b***) and due to uncontrolled growth of fire in abandoned, unreclaimed fire-affected sites (***c***).

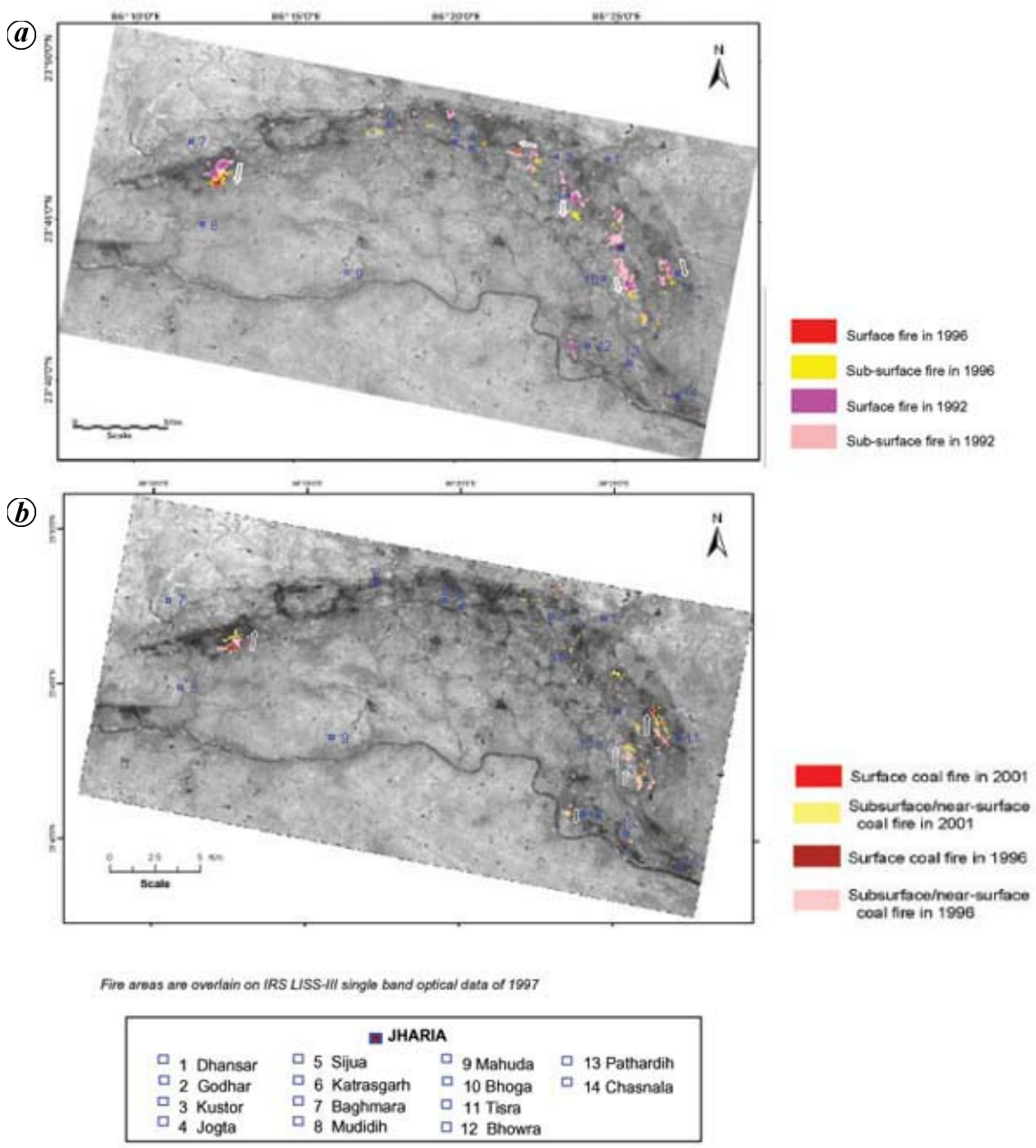

Figure 9. Lateral propagation of coal fire during 1992–96 (***a***) and 1996–2001 (***b***). Individual coal-fire areas of 1992, 1996 and 2001 prepared from Landsat TM and ETM+ data are overlain on IRS LISS-III single-band image. (Arrows indicate lateral propagation directions during the observation periods.)

tween discrete observations. Large time series data are therefore essential for studying coal-fire propagation. In this study, an attempt was made to find the net lateral propagation of coal fire during 1992–96 and 1996–2001 from three datasets (Figure 9). It is observed that during 1992–96, the net lateral propagation of coal-fire was in general towards south and at places towards west. On the other hand, during 1996–2001, it was in general towards north, except at a few places such as near Bhowra Township where it was towards south. Propagation of coal fire was therefore found to be more erratic than regular in nature. Extensive study on spatial disposition of the affected and neighbouring coal seams; density, alignment and depth consistency of the fractures and faults; use of a large time series satellite data, and due consideration to meteorological parameters such as incidence of rain, wind

speed and direction at the time of satellite data acquisition will help obtain sufficiently accurate lateral coal fire propagation direction.

Conclusion

In this study, medium resolution night- and day-time satellite TIR data and night-time SWIR data of multiple dates were used efficiently for studying the dynamics of coal fire in Jharia Coalfield. The dynamics of coal fire was studied in terms of changes in spatial extent of fire-affected areas and propagation of coal fire. Initially, from the raw digital data, spectral radiance at each ground resolution cell or pixel was calculated using the scene-specific calibration parameters instead of the standard calibration parameters, as listed in the literature[1]. From the spectral radiance values, radiant temperature was calculated using Planck's radiation equation and subsequently kinetic temperature considering thermal emissivity at each pixel. Thermal emissivity image was generated based on NDVI values in vegetation-covered areas and from a knowledge of the spectral absorption properties of surface cover in remaining areas. Subsequently, surface and subsurface coal-fire areas were delineated from the respective kinetic temperature images using field-based threshold temperatures. Besides, from the night-time SWIR band data (Landsat-5 TM band 7), surface coal-fire locations were pinpointed.

From the multi-date coal-fire maps prepared from TIR data, it is observed that the total fire-affected area was reduced substantially from 2.49 sq. km in 1992, to 1.70 sq. km in 1996 and to 1.59 sq. km in 2001. Of this, surface coal fire shared 0.42, 0.33 and 0.08 sq. km in 1992, 1996 and 2001 respectively, and the rest 2.06, 1.36 and 1.60 sq. km were shared by subsurface coal fire in 1992, 1996 and 2001 respectively. An attempt was also made to find the net lateral propagation of coal fire from multi-date TIR data. It is observed that during 1992–96, the net lateral propagation of coal fire was in general towards south and at places towards west, whereas during 1996–2001, it was in general towards north, except at a few places where it was towards south as well. The study on the propagation of coal fire requires more detailed analysis on three-dimensional disposition of the affected and neighbouring coal seams; density, alignment and depth consistency of fractures and faults, as well as the use of a large time-series satellite data with dense temporal sampling, giving due consideration to meteorological parameters such as incidence of rain, wind speed and wind direction at the time of satellite data acquisition.

1. Markham, B. L. and Barker, J. L., EOSAT Landsat Technical Notes 1. Earth Observation Satellite Co, Maryland, August 1986, pp. 3–8.
2. Prakash, A., Saraf, A. K., Gupta, R. P., Dutta, M. and Sundaram, R. M., *Int. J. Remote Sensing*, 1995, **16**, 2105–2109.
3. Saraf, A. K., Prakash, A., Sengupta, S. and Gupta, R. P., *Int. J. Remote Sensing*, 1995, **16**, 2111–2124.
4. Prakash, A., Gupta, R. P. and Saraf, A. K., *Int. J. Remote Sensing*, 1997, **18**, 2463–2469.
5. Zhang, X., Van Genderen, J. L. and Kroonenberg, S. B., *Int. J. Remote Sensing*, 1997, **18**, 3279–3288.
6. Chatterjee, R. S., *ISPRS J. Photogramm. Remote Sensing*, 2006, **60**, 113–128.
7. Reddy, C. S. S., Srivastav, S. K. and Bhattacharya, A., *Int. J. Remote Sensing*, 1993, **14**, 3125–3132.
8. Prakash, A. and Gupta, R. P., *Int. J. Remote Sensing*, 1999, **20**, 1935–1946.
9. Richter, R., *Int. J. Remote Sensing*, 1990, **11**, 159–166.
10. Mansor, S. B., Cracknell, A. P., Shilin, B. V. and Gornyi, V. I., *Int. J. Remote Sensing*, 1994, **15**, 1675–1685.
11. Barsi, J. A. *et al.*, *Can. J. Remote Sensing*, 2003, **29**, 141–153.
12. Kneizys, F. S. *et al.*, AFGL-TR-88-0177, Air Force Geophysics Lab., Hanscomb AFB, Massachusetts, USA, 1988.
13. Van de Griend, A. A. and Owe, M., *Int. J. Remote Sensing*, 1993, **14**, 1119–1131.
14. Buettner, K. J. K. and Kern, C. D., *J. Geophys. Res.*, 1965, **70**, 1329–1337.
15. *Mem. Geol. Surv. India*, 1964, **84**, Plate 6.

ACKNOWLEDGEMENTS. We thank Mr R. V. Erady, formerly BCCL for his interest, help and cooperation. We also thank Dr P. S. Roy, National Remote Sensing Agency (NRSA), Hyderabad and Prof. V. K. Jha, formerly Indian Institute of Remote Sensing, NRSA, Dehradun for help, support and encouragement. We acknowledge the help and cooperation from the officials and staff of BCCL. We thank the two anonymous reviewers for their suggestions and comments which helped improve the manuscript.

Received 23 March 2006; revised accepted 26 August 2006